Lawrence Berkeley Laboratory
UNIVERSITY OF CALIFORNIA

Materials & Molecular
Research Division

Submitted to the Journal of Nuclear Materials

OXYGEN DIFFUSION IN UO_{2-x}

K.C. Kim and D.R. Olander

April 1981

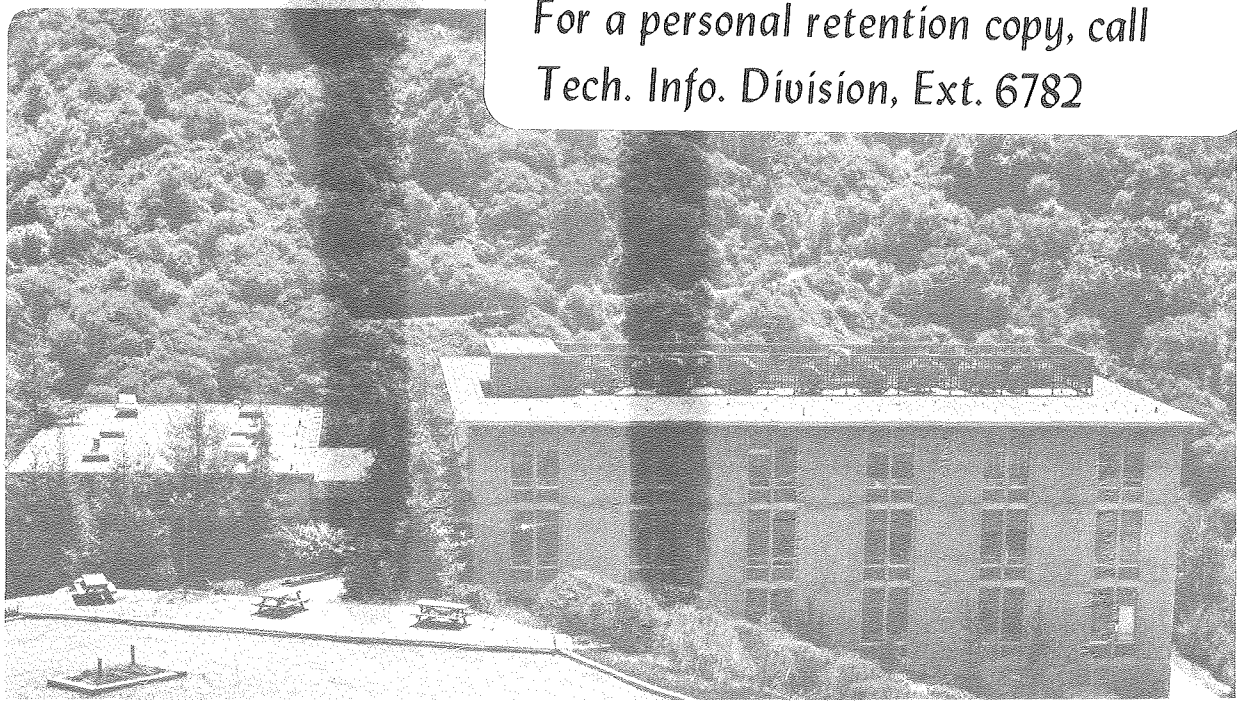

Prepared for the U.S. Department of Energy under Contract W-7405-ENG-48

DISCLAIMER

LBL-12624

OXYGEN DIFFUSION IN UO_{2-x}

K. C. Kim
and
D. R. Olander

Materials and Molecular Research Division
Department of Nuclear Engineering
Lawrence Berkeley Laboratory
University of California
Berkeley, California 94720

Submitted to J. Nuclear Materials

This work was supported by the Director, Office of Energy Research, Office of Basic Energy Sciences, Materials Sciences Division of the U.S. Department of Energy under contract # W-7405-ENG-48.

ABSTRACT

The tracer oxygen diffusivity in UO_{2-x} has been measured along the lower two-phase boundary. The diffusion couple consisted of two matched hypostoichiometric uranium dioxide wafers, one enriched with ^{18}O and the other normal, pressed together with a bond of liquid uranium in between. Oxygen-18 concentration profiles were determined by ion microprobe mass analysis, from which diffusion coefficients were obtained. Activation energy of anion vacancy migration was found to be 11.7 ± 3.0 kcal/mole. A diffusion model for $UO_{2\pm x}$ showed that both interstitials and vacancies contribute significantly to oxygen diffusion in stoichiometric UO_2. The Frenkel defect energy and entropy of 85.6 ± 9.2 kcal/mole and 18.2 ± 7.2 e.u., respectively were deduced from the model. Using these values, the contribution of Frenkel disorder to the excess enthalpy of UO_2 was evaluated. A simple two-band model for electronic excitation, with a band gap of 2.0 ev and effective electron mass of 7.6 m_e, accounted for the remainder of the excess enthalpy.

I INTRODUCTION

Transport phenomena in the heavy metal oxides are of importance in understanding the behavior of fuel elements during reactor operation. Oxygen diffusion is of special interest because of the influence of the oxygen-metal ratio on the fundamental properties of the oxide. There have been many studies, both theoretical and experimental, of oxygen diffusion in stoichiometric UO_2 and UO_{2+x} [1-11]. Oxygen diffusion in isostructural oxides CeO_{2-x} [12,13] and PuO_{2-x} [14,15] has also been investigated. However, similar measurements in hypostoichiometric urania have never been attempted, mainly because UO_{2-x} is a defect structure stable only at high temperatures so that its oxygen diffusion coefficient may be large enough to render conventional methods unworkable. For example, in the gas-solid isotopic exchange method [2,7], the gas phase mass transfer step or the surface isotopic exchange step may be rate-controlling. Also, since the equilibrium oxygen potential of hypostoichiometric uranium dioxide is extremely low, it would be very difficult to control the gas stream to maintain stoichiometry during the diffusion anneal. Even if this could be achieved, it is doubtful that this small oxygen potential could be successfully isotopically monitored for diffusion measurements. These problems were solved by the use of a solid-solid diffusion couple.

Together with thermodynamic information, transport data contribute to the understanding of the defect structure of uranium dioxide. Oxygen diffusion studies in CeO_{2-x} and PuO_{2-x} gave vacancy migration energies in the range of 4-12 kcal/mole, which may be compared with 21-23 kcal/mole for interstitial migration energy in UO_{2+x}. In addition, Catlow et al. [16] theoretically determined a value of 5.8 kcal/mole for vacancy

migration in UO_{2-x}. Using this estimate, Murch and Thorn [9] calculated the diffusion coefficient of oxygen in $UO_{2\pm x}$ assuming mobility of both interstitials and vacancies. Nevertheless, there remains considerable uncertainty concerning the fundamental aspects of the defect properties and transport mechanisms in urania. The main difficulty is the lack of oxygen diffusion data in UO_{2-x}.

II EXPERIMENTAL METHOD

The diffusion couple consisted of two UO_{2-x} wafers, one of which was enriched with ^{18}O. Although many of the problems associated with the gas-solid exchange method are avoided, the solid-solid technique has the difficulty in achieving good contact between the two wafers. If a gas or vacuum gap separates the two wafers, calculation shows that the vapor pressure of UO_2 is too low for sufficient oxygen transport from one side to another. To avoid this interfacial resistance, the wafers were bonded together by liquid uranium. Liquid uranium is believed to have a sufficiently high oxygen solubility [17-20] so that the liquid metal bond should transport oxygen from one wafer to the other quite efficiently. This technique is equivalent to reduction of the heat transfer resistance in the fuel-cladding gap of carbide fuel pins by sodium bonding.

To avoid perturbing the stoichiometry of the oxide by the liquid uranium band, the experiments were performed with wafers in the $U(\ell)+UO_{2-x}$ two-phase region. The stoichiometry was thus fixed automatically by the temperature and therefore the diffusion measurements represented conditions along the lower phase boundary of the U-O system. The presence of a small amount of liquid uranium in the

oxide served to buffer the composition of the latter against changes due to oxygen gain or loss to the environment during testing.

The surfaces of two wafers of sintered uranium dioxide 1 mm thick and 1.17 mm diameter or single crystals of the same dimensions were polished using silicon carbide powder and diamond paste. Enrichment of one wafer in oxygen-18 was accomplished by contact with flowing hydrogen saturated with $H_2{}^{18}O$ for 15 hrs at 1500 °C in the apparatus shown in Fig. 1. For the isotope enrichment process, valves 1 and 2 were open and valves 3 and 4 were closed. The weight gain of the sample during this treatment was used to monitor the enrichment process, which produced oxygen-18 fractions in the solid ranging from 0.5 to 0.8. To provide a matched wafer of normal UO_2, the same procedure was followed using normal water instead of $H_2{}^{18}O$ in the saturator.

For stoichiometry control, the set of matched wafers (one $U^{16}O_2$ and the other $U^{18}O_2$) along with a third wafer to be used for stoichiometry determination were placed in the furnace of Fig. 1. The wafers were separated as far as possible to minimize premature isotope exchange of oxygen by gas phase transfer. The samples were then exposed to purified hydrogen at 2000 °C for 4 hours with valves 1 and 2 closed and 3 and 4 open. The final O/U ratio of the specimens (determined by measuring the weight gain of the third wafer in an H_2O/H_2 mixture selected to return the oxygen-to-uranium ratio to 2.00) was $\sim$ 1.95. As a result of the isotopic exchange and reduction processes, the grain size of the specimens was $\sim$ 200 μm and metallic uranium was visible under the microscope in the room-temperature specimens.

Following the preparatory steps described above, the reduced wafers, one of which was enriched in oxygen-18, were placed together with a 75 μm-thick foil of uranium metal in between. This sandwich

was placed in a molybdenum holder and lid, with rhenium foils to prevent direct contact of the specimen with the crucible (Fig. 2). The assembly was installed in a resistance furnace and weight placed on the molybdenum lid to promote good contact between the two wafers. The system was slowly heated to 1100 °C in flowing purified helium. Once the uranium metal melted (1132 °C) heating to operating temperature was rapid (less than 2 min). The temperature was maintained for the desired annealing time (15 - 350 min). After rapid cooling, the couple was taken out of the furnace and cut perpendicular to the interface. Each part was mounted in conductive epoxy and polished. The $^{18}O/(^{18}O + ^{16}O)$ distribution through the two wafers was determined by ion microprobe analysis.

Ten experiments using sintered uranium dioxide specimens in the temperatures range from 1200 to 1600 °C were conducted. According to Fryxell's[21] equation for the lower phase boundary of UO_{2-x},

$$\ln x = 3.678 - 12675/T(K),$$

this temperature range corresponds to oxide stoichiometries from 1.955 to 1.993. Several experiments were also conducted using single crystal wafers.

Additional experimental details are given in Ref. 22.

III RESULTS

Figure 3 shows the state of the interface between the enriched and normal wafers following a diffusion anneal for 30 min at 1400 °C. Despite the low temperature (for sintering in UO_2), completely healed sections of the gap can be seen. A coherent bond of uranium metal $\sim$ 5 μm thick fills the remainder of the interface. The oxygen-18 distribution was determined by ion microprobe analysis along lines

perpendicular to the interface. One trace was made along the axis and another mid-way between the center and the periphery. Figure 4 shows the results of the analysis at two temperatures. The ordinate represents the normalized concentration:

$$\phi = \frac{y - y_0}{y_1 - y_0} \tag{1}$$

where y is the isotopic fraction of oxygen-18 and y_0 and y_1 are the initial values for the normal and enriched wafers, respectively. These fractions were readily measurable in the regions of the wafers farthest from the interface which were unaffected by isotopic exchange by solid state diffusion.

The results for the 1257 °C anneal exhibit a discontinuity at the interface, which indicates that the gap was a significant resistance to transport of oxygen. By 1400°C, the gap had vanished. Both profiles are symmetric about the interface. The tracer diffusion coefficient of oxygen can be determined even in the presence of an appreciable gap resistance such as that seen in the upper curve of Fig. 4. To determine the diffusivity from the measured profiles, Fick's second law must be solved:

$$\frac{\partial \phi}{\partial \tau} = \frac{\partial^2 \phi}{\partial \eta^2} \tag{2}$$

where ϕ is given by Eq(1), $\tau = Dt/\ell^2$ is the dimensionless time and $\eta = z/\ell$ is the dimensionless distance. ℓ is the thickness of a wafer. The initial conditions are:

$$\phi(\eta, 0) = \begin{cases} 1 \text{ for } 0 \leqslant \eta \leqslant 1 \\ 0 \text{ for } 1 \leqslant \eta \leqslant 2 \end{cases} \tag{3}$$

The boundary conditions at the outer surfaces are:

$$\partial\phi/\partial\eta = 0 \text{ at } \eta = 0 \text{ and } \eta = 2 \qquad (4)$$

The conditions at the interface represent transport through the uranium liquid layer of half-thickness δ and equality of the oxygen fluxes on either side of the interface (22):

$$\begin{aligned} \partial\phi/\partial\eta &= -B(\phi - 0.5) \qquad \text{at } \eta = 1^- \\ \partial\phi/\partial\eta &= -B(0.5 - \phi) \qquad \text{at } \eta = 1^+ \end{aligned} \qquad (5)$$

where B is a parameter representing the overall conductance of the uranium layer for oxygen:

$$B = \frac{D_U}{D} \frac{\ell}{\delta} \frac{C_O^U}{C_O} \qquad (6)$$

In this equation, D_U and D are the diffusivities of oxygen in liquid uranium and in solid UO_{2-x}, respectively, C_O^U is the solubility of oxygen in liquid uranium and C_O is the concentration of oxygen in UO_{2-x}. The parameter B is a permeability ratio; the larger its value, the smaller is the oxygen-transport resistance of the uranium bond.

Equation (2) subject to the conditions of Eqs(3) - (5) can be solved analytically [23]. In real time and position, the solution is:

$$\phi = \frac{1}{2} + \sum_{n=1}^{\infty} e^{-D\beta_n^2 t} \frac{\{(\ell\beta_n)^2 + B^2\}\cos(\beta_n z)}{\{(\ell\beta_n)^2 + B^2 + B\}} \frac{\sin(\beta_n \ell)}{\beta_n \ell} \qquad (7)$$

The β_n's are positive roots of $(\beta\ell)\tan(\beta\ell)-B=0$. The best values of D and B were sought to fit the data points from the diffusion experiments to Eq(7). Small corrections for the heat up and cool-down times were also made [22].

Along the lower phase boundary, the primary source of oxygen mobility is the vacancy mechanism, for which the self-diffusion coefficient is [24]:

$$D \simeq D_V = A_V \theta_V (1-\theta_V) \exp(-\Delta H_V/RT) \qquad (8)$$

The activation energy of vacancy migration is ΔH_V and A_V is the pre-exponential factor. The anion vacancy concentration (site fraction) is denoted by θ_V. Since thermally-generated vacancies are negligible compared to extrinsic vacancies arising from the deviation from stoichiometry in UO_{2-x}, the condition $\theta_V = x/2$ applies to the experimental diffusivities. In Fig. 5 the diffusivities determined from data such as those shown in Fig. 4 are plotted in the Arrhenius form suggested by Eq(8). The constants determined from the best-fitting line are $A_V = 4.4 \times 10^{-4}$ cm^2/s and $\Delta H_V = 11.7 \pm 3.0$ kcal/mole. The diffusion coefficients measured in single crystal specimens fall about 20% below those for the polycrystalline material shown in Fig. 5.

IV DISCUSSION

A. Diffusion Mechanism in UO_{2-x}

Due to the similarity in crystal structure, it has been widely believed that UO_{2-x} has the same type of crystal defect (anion vacancy) and diffusion mechanism (vacancy) as CeO_{2-x} and PuO_{2-x}. On the other hand, thermodynamic studies favor the excess uranium model [25]. Since stoichiometry and temperature were changed simultaneously in the present experiment, unequivocal separation of

the two contributions was not possible. However, the present diffusion coefficients for UO_{2-x} are almost two orders of magnitude higher than those of stoichiometric UO_2 (1), which suggests the dominance of oxygen vacancies in UO_{2-x}. Moreover, Fig. 5 shows that the predicted composition dependence of the vacancy mechanism is consistent with the data.

Experimental results on CeO_{2-x} and PuO_{2-x} are compared with the present work in Table 1. It is seen that both the activation energies and pre-exponential factors are in excellent agreement with those of CeO_{2-x} and PuO_{2-x}. The current model is based on random walk theory with no interactions among defects, which is valid only for small nonstoichiometries. Therefore, the disagreement in Table 1 between $CeO_{1.80}$ and the remaining values is attributed to the large deviation in the stoichiometry of the former, which gives rise to defect clustering or microdomains of ordered structures [12].

B. Oxygen Diffusion in Near-Stoichiometric $UO_{2\pm x}$

Having measured the transport properties of anion vacancies in UO_{2-x}, re-analysis of oxygen diffusion in $UO_{2\pm x}$ is in order. The basis of the analysis, as implemented by Breitung [8] and Murch and Thorn [9], includes: i) consideration of thermally-generated (intrinsic) point defects as well as those required by nonstoichiometry (extrinsic), and ii) addition of transport due to independently-operating vacancy and interstitialcy mechanisms.

The concentrations of thermally generated point defects are governed by the anion Frenkel equilibrium:

$$O_o + V_i \overset{\rightarrow}{\leftarrow} V_o + O_i$$

where O_o denotes an oxygen ion in a regular lattice site,

V_i an unoccupied interstitial site,

O_i an oxygen ion in an interstitial site, and

V_o a vacancy in a regular lattice site.

The site fraction of vacancies (θ_v) and of interstitials (θ_i) are related by the law of mass action:

$$K_F = \left(\frac{\theta_v}{1-\theta_v}\right)\left(\frac{\theta_i}{1-\theta_i}\right) = \exp(\Delta S_F/R)\exp(-\Delta H_F/RT) \qquad (9)$$

where ΔS_F and ΔH_F are the entropy and enthalpy, respectively, of anion Frenkel defect formation. The number of available anion interstitial sites in UO_2 and UO_{2-x} is equal to number of uranium atoms. In UO_{2+x}, however, the concentration of occupiable interstitial sites (α) decreases. Contamin et al. [3] propose the semi-empirical expression:

$$\alpha = \begin{cases} 1 & \text{for } UO_{2-x} \\ 2\left\{(2+x)(1+10^3x^3)^{\frac{1}{2}}\right\}^{-1} & \text{for } UO_{2+x} \text{ and } UO_2 \end{cases} \qquad (10)$$

Finally, electrical neutrality provides the condition:

$$x = \alpha\theta_i - 2\theta_v \qquad (11)$$

Simultaneous solution of Eqs(9) - (11) gives the point defect concentration θ_i and θ_v as a function of temperature and stoichiometry provided that the thermodynamic properties of the Frenekel equilibrium are known.

In accord with the second assumption given at the beginning of

this section, the self-diffusion coefficient of oxygen in $UO_{2\pm x}$ is the sum of contributions from vacancy and interstitialcy mechanisms:

$$D = D_V + D_i \tag{12}$$

where D_V is given by Eq(8) and D_i by [3]:

$$D_i = A_i\theta_i(1-\theta_i)\exp(-\Delta H_i/RT) \tag{13}$$

where A_i and ΔH_i are the pre-exponential factor and activation energy, respectively, for interstitial migration. In substantially hyper-stoichiometric UO_{2+x}, $\theta_i \simeq x/\alpha$ and $\theta_V \simeq 0$. Based upon these conditions, the data of Contamin et. al.[3] and Murch[6] were fitted to Eq(13) to yield $A_i = 4.7\times10^{-3}$ cm^2/s and $\Delta H_i = 21.8 \pm 13.0$ kcal/mole.

For $UO_{2.00}$, $\alpha = 1$ and $x = 0$, so that $\theta_i = 2\theta_V$. The point defect concentrations can be calculated from Eq.(9) for selected values of ΔS_F and ΔH_F. With A_V, ΔH_V, A_i and ΔH_i known, the diffusion coefficient was calculated as a function of temperature from Eqs(8), (12) and (13). The best fit of the calculation to the diffusion measurements in stoichiometric UO_2 by Marin and Contamin[1] were used to determine the Frenkel entropy and enthalpy. The "transport-based" values so determined are

$$\Delta H_F = 85.6 \pm 9.2 \text{ kcal/mole and } \Delta S_F = 18.2 \pm 7.2 \text{ e.u.}$$

These may be compared with the "thermal-based" values $\Delta H_F = 71.3 \pm 2.2$ kcal/mole and $\Delta S_F = 14.8 \pm 0.8$ e.u. The latter were determined by Swarc[26] by assuming that Frenkel disorder was the sole cause of the "excess" specific heat of UO_2. As a corollary of the data-fitting process, the contributions of D_V and D_i to oxygen self-diffusion in stoichiometric UO_2 are obtained. At low temperatures, vacancies are the primary species contributing to oxygen mobility in UO_2. Between

800 and 1800 °C, both point defects possess significant mobility; D_i and D_v are calculated to be equal at 1400 °C. Interstitials predominate at very high temperatures.

The diffusivities of oxygen in UO_{2-x} from the present analysis are two to three orders of magnitude smaller than those calculated by Murch and Thorn [9], which were based on too low a value of ΔH_v.

C. ELECTRONIC EXCITATION

As indicated in the preceding section, the specific heat of UO_2 displays an unusually rapid increase at temperatures above $\sim$ 1800°C [27-30]. Szwarc [26] attributed all of this "excess" enthalpy to Frenkel disorder, but recently, the phenomenon has been re-interpreted in terms of electronic excitation [31-33]. Because the "transport-based" point defect thermodynamic properties were deduced independently of the thermal properties of the solid, it is possible to quantitatively estimate the contributions of atomic and electronic disorder to the excess enthalpy. The latter is:

$$\Delta H_{ex} = \Delta H_{Fr} + \Delta H_{el} \qquad (14)$$

Kerrisk et. al. [30] determined an accurate representation of the phonon contribution which, when subtracted from the total enthalpy at temperatures above $\sim$ 1800 °C [28, 29] provides "experimental" values of ΔH_{ex} as a function of temperature. The Frenkel disorder term in Eq(14) is[26]:

$$\Delta H_{Fr} = \sqrt{2}\ \Delta H_F \exp\left(\frac{\Delta S_F}{2R}\right) \exp\left(-\frac{\Delta H_F}{2RT}\right) \qquad (15)$$

MacInnes [31] calculated the electronic contribution by using the two-band structure with a band gap of E_g. Using standard techniques of semiconductor theory, the energy absorbed by the band structure

can be computed. Using Thorn's [32] assignment of 5f orbitals for the valence band, the electronic contribution to the excess enthalpy becomes:

$$\Delta H_{el} = \left(\frac{m^*}{m_e}\right)^{3/4} [1.789 \times 10^{-3} T^{7/4} + 6.003 \times 10^{-4} E_g \cdot T^{3/4}] \exp(- E_g/2RT) \qquad (16)$$

where m^*/m_e is the ratio of the effective and rest masses of the electron. Using the "transport-based" values of ΔS_F and ΔH_F in Eq(15), m^*/m_e and E_g in Eq(16) were chosen to provide the best fit to the excess enthalpy data. This procedure yields $m^*/m_e = 7.6 \pm 0.1$ and $E_g = 45 \pm 1$ kcal/mole. The latter figure is in good agreement with the band gap energies in UO_2 deduced from electrical conductivity measurements (1.8 - 2.3 ev, Ref. 34) and from optical reflectivity data (2.1 eV, Ref. 35). The electronic enthalpy ΔH_{el} and the Frenkel enthalpy ΔH_{Fr} are calculated separately and shown in the lower graph. Their fractional contributions to the excess enthalpy are shown in the upper graph. As temperature increases the fraction of electronic excitation decreases, accounting for approximately 13 percent of the total excess enthalpy at 3000 K. This behavior arises from the different temperature dependences of the two terms in Eq(14); Frenkel disorder increases with temperature according to an enthalpy of formation of $\sim$86 kcal/mole whereas electronic excitation is thermally activated by a band gap energy just over one half of this value.

V. CONCLUSIONS

1. Oxygen diffusion in UO_{2-x} is much faster than in UO_2 consistent with the anion vacancy as the primary defect in UO_{2-x}.
2. The measured activation energy of the anion vacancy migration (11.7 kcal/mole) is lower than that of interstitials, but not as low as that predicted by theoretical calculation. The activation energy and the pre-exponential factor of the oxygen diffusion coefficient are in good agreement with those of other oxides of fluorite structure, e.g., CeO_{2-x}, PuO_{2-x}.
3. Both vacancies and interstitials contribute significantly to oxygen diffusion in stoichiometric UO_2. At 1400 °C, contributions of the two species are approximately equal.
4. The Frenkel energy and entropy deduced from measured diffusivities in UO_{2-x}, UO_2 and UO_{2+x} are 85.6 kcal/mole and 18.2 e.u., respectively.
5. Not all of the excess enthalpy of UO_2 can be attributed to Frenkel disorder. Use of the ΔH_F and ΔS_F values determined in this study and the two-band model of electronic excitation yields a band gap of 2.0 eV. Electronic excitation accounts for $\sim$ 13 percent of the excess enthalpy at 3000 K.

ACKNOWLEDGEMENT

This work was supported by the Director, Office of Energy Research, Office of Basic Energy Sciences, Materials Sciences Division of the U.S. Department of Energy under contract # W-7405-ENG-48.

Table 1. Comparison of oxygen diffusion in UO_{2-x} with that in CeO_{2-x} and PuO_{2-x}

X	CeO_{2-x}[12,13]	PuO_{2-x}[15]	UO_{2-x} (this work)
0.005	-	$0.2\times10^{-5}\exp(-10900/RT)$	$0.11\times10^{-5}\exp(-11700/RT)$
0.01	-	$0.5\times10^{-5}\exp(-11100/RT)$	$0.22\times10^{-5}\exp(-11700/RT)$
0.03	-	$1.3\times10^{-5}\exp(-11300/RT)$	$0.65\times10^{-5}\exp(-11700/RT)$
0.05	-	$1.6\times10^{-5}\exp(-10800/RT)$	$1.07\times10^{-5}\exp(-11700/RT)$
0.08	$1.51\times10^{-5}\exp(-11900/RT)$	-	$1.68\times10^{-5}\exp(-11700/RT)$
0.2	$6.16\times10^{-6}\exp(-3600/RT)$	-	-

REFERENCES

1. J.F. Marin and P. Contamin, J. Nucl. Mater., 30 (1969) 16.
2. A.B. Auskern and J. Belle, J. Nucl. Mater., 3 (1961) 267.
3. P. Contamin, J.J. Backmann, and J.F. Marin, J. Nucl. Mater., 42 (1972) 54.
4. J. Belle, J. Nucl. Mater., 30 (1969) 3.
5. G.E. Murch, Phil. Mag., 32 (1975) 1129.
6. G.E. Murch, D.H. Bradhurst, and H.J. de Bruin, Phil, Mag., 32 (1975) 1141.
7. L.E. Roberts, V.J. Wheeler, and A. Perrin, 1969, unpublished work cited by J. Belle, J. Nucl. Mater., 30 (1969) 3.
8. W. Breitung, J. Nucl. Mater., 74 (1978) 10.
9. G.E. Murch and R.J. Thorn, J. Nucl. Mater., 71 (1978) 219.
10. R.J. Thorn and G.H. Winslow, "Thermodynamics of Nuclear Materials", IAEA, Vienna (1965).
11. P. Contamin, 1971, Doctoral Dissertation, University of Grenoble, CEA-A-4228.
12. J.M. Floyd, Ind. J. of Tech., 11 (1973) 589.
13. B.C.H. Steele and J.M. Floyd, Proc. Brit. Ceram. Soc. 19 (1971) 55.
14. P. Chereau and J.F. Wadier, J. Nucl. Mater., 46 (1973) 1.
15. A.S. Bayoglu and R. Lorenzelli, J. Nucl. Mater., 82 (1979) 403.
16. C.R.A. Catlow and A.B. Lidiard, "Thermodynamics of Nuclear Materials," IAEA, Vienna (1974), Vol. 3, p27.
17. A.E. Martin and R.K. Edwards, J. Phys. Chem., 69 (1965) 1788.
18. R.K. Edwards and A.E. Martin, "Thermodynamics of Nuclear Materials", IAEA, Vienna (1965) vol 2, p423.

19. P. Guinet, H. Vaugoyeau and P.L. Blum, CEA-Report-3060, (1966).

20. S.P. Garg and R.J. Ackermann, J. Nucl. Mater., 88 (1980) 309.

21. R.E. Fryxell, D.E. Joyce, and R. Szwarc, J. Nucl. Mater., 25 (1968) 97.

22. K.C. Kim, "Oxygen Diffusion in Hypostoichiometric Uranium Dioxide", LBL-11905 (1980).

23. H.S. Carslaw and J.C. Jaeger, "Conduction of Heat in Solids," 2nd Ed., Oxford, Claredon Press (1959).

24. M. O'Keefe, "Chemistry of Extended Defects in Non-Metallic Solids," L. Eyring and M. O'Keefe Ed., North-Holland (1970).

25. P. Kofstad, "Nonstoichiometry, Diffusion and Electrical Conductivity in Binary Metal-oxides," Wiley-Interscience (1972).

26. R. Szwarc, J. Phys. Chem. Solids, 30 (1969) 705.

27. A.E. Ogard and J.A. Leary, "Thermodynamics of Nuclear Materials," IAEA, Vienna (1967).

28. R.A. Hein, L.H. Sjodhl, and R. Szwarc, J. Nucl. Mater., 25 (1968) 99.

29. L. Leibowitz, L.W. Mishler, and M.G. Chasanov, J. Nucl. Mater., 29 (1969) 356.

30. J.F. Kerrisk and D.G. Clifton, Nucl. Technol., 16 (1972) 531.

31. D.A. MacInnes, J. Nucl. Mater., 78 (1978) 225.

32. R.J. Thorn, G.H. Winslow, and J.S. Ziomek, J. Nucl. Mater., 87 (1979) 416.

33. D.A. MacInnes and C.R.A. Catlow, J. Nucl. Mater., 89 (1980) 354.

34. J.L. Bates, C.A. Hinman, and T. Kawada, J. Am. Ceram. Soc., 50 (1967) 652.

35. J. Schoenes, J. Appl. Phys., 49 (1978) 1463.

FIGURE CAPTIONS

Figure 1. Flow diagram of the system for enriching UO_2 in oxygen-18 or for stoichiometry control.

Figure 2. Diffusion couple arrangement.

Figure 3. Interface between the two UO_{2-x} wafers showing the uranium metal band. Annealed for 30 min. at 1400°C.

Figure 4. Ion microprobe profiles of oxygen-18 fraction through the diffusion couple; □ - along axis; Δ - halfway between center and edge.

Figure 5. Plot of polycrystalline diffusivity data in UO_{2-x} in the form suggested by Eq.(7); $\theta_v = x/2$.

Figure 6. Absolute and fractional contributions of Frenkel disorder and electronic excitation to the excess enthalpy in UO_2.

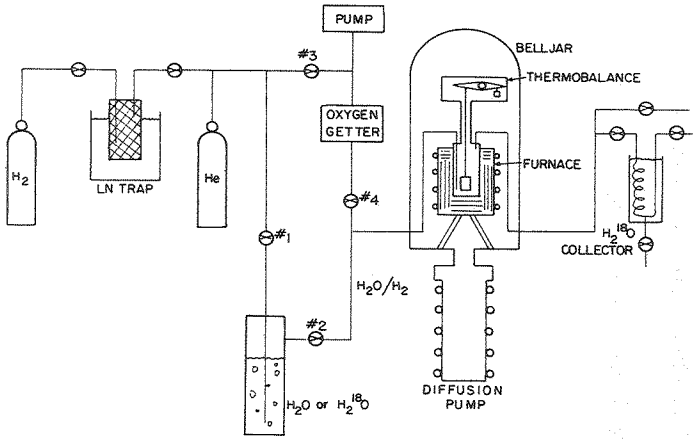
PUMP
#3
BELLJAR
THERMOBALANCE
OXYGEN GETTER
FURNACE
H_2
LN TRAP
He
#4
#1
H_2O/H_2
$H_2^{18}O$ COLLECTOR
#2
H_2O or $H_2^{18}O$
DIFFUSION PUMP
XBL 8010-6097

Fig. 1

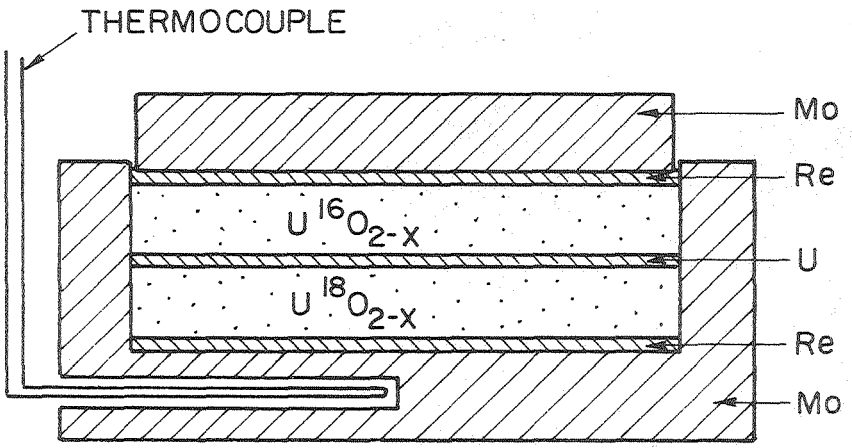

XBL 8010-6086

Fig. 2

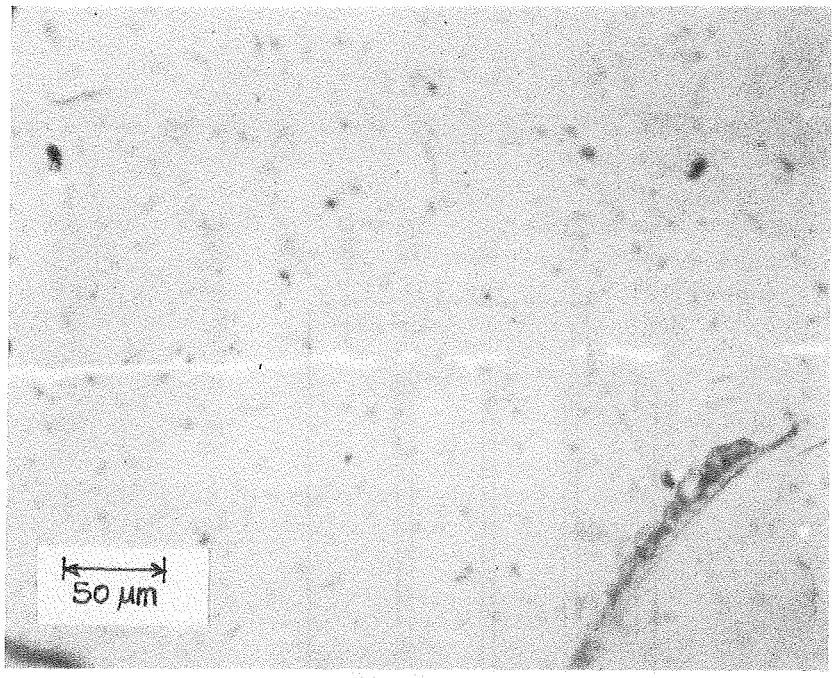

Fig. 3 XBB8010-11799

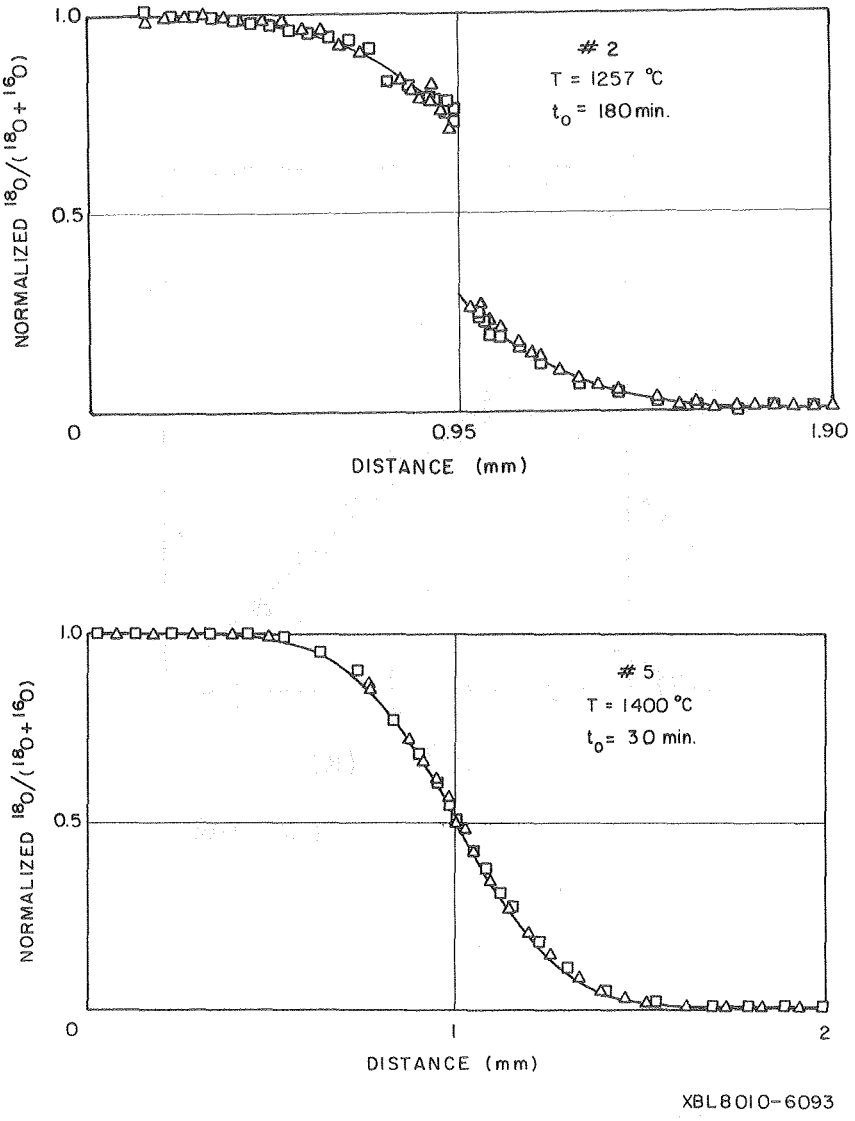
1.0
0.5
0
NORMALIZED $^{18}O/(^{18}O+^{16}O)$
# 2
T = 1257 °C
t_o = 180 min.
0.95
1.90
DISTANCE (mm)
1.0
0.5
0
NORMALIZED $^{18}O/(^{18}O+^{16}O)$
# 5
T = 1400 °C
t_o = 30 min.
1
2
DISTANCE (mm)
XBL8010-6093

Fig. 4.

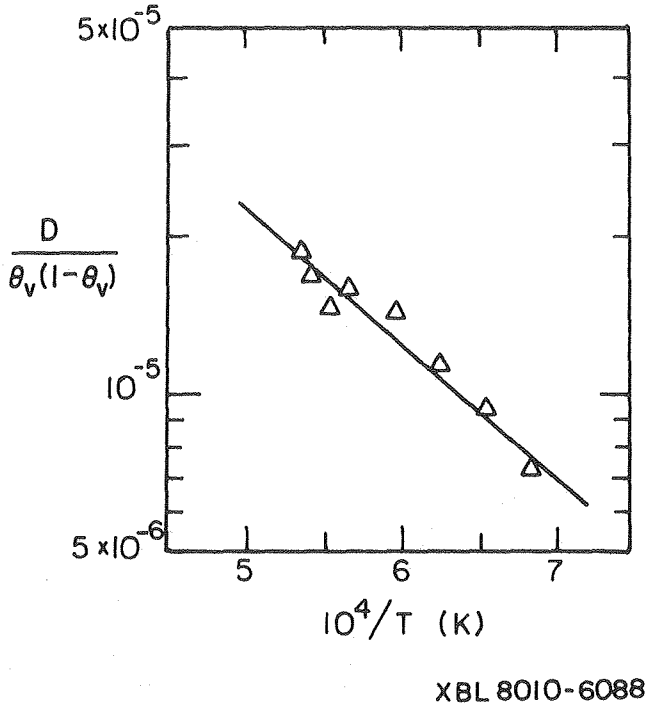

Fig. 5

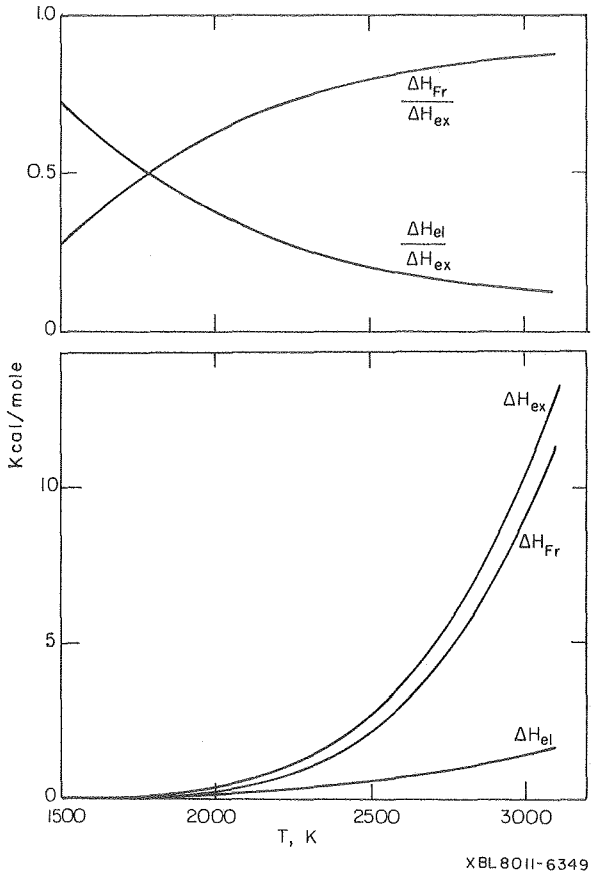
1.0
0.5
0
$\frac{\Delta H_{Fr}}{\Delta H_{ex}}$
$\frac{\Delta H_{el}}{\Delta H_{ex}}$
Kcal/mole
10
5
0
ΔH_{ex}
ΔH_{Fr}
ΔH_{el}
1500
2000
2500
3000
T, K
XBL8011-6349

Fig. 6